A Challenging and Promising Effort toward QNDE for Inaccessible and Invisible Defects; Nonlinear Guided Wave NDE

Weibin Li[1] and Younho Cho[2, a]

[1]School of Aerospace Engineering, Xiamen University, Xiamen, 361005, China
[2]School of Mechanical Engineering, Pusan National University, Busan, 609-735, Korea

[a)] mechcyh@pusan.ac.kr

Abstract: The use of ultrasonic guided wave, which has been widely accepted as a conventional、 screening NDE tool to overcome the inaccessibility of large scale structural integrities is now being extended to early stage damage detection in conjunction with its nonlinear features for more precise material characterization. The status of guided wave based NDE is evolved from detecting geometric defects to monitoring strength related ones. Combining guided wave based NDE schemes with its nonlinearity is challenging due to the existence of multiple modes, the dispersive manner and the need of proper mode tuning. In this paper, some key concepts for the success will be introduced along with recent accomplishments including nonlinear guided wave imaging and application to composites.
**Keywords:** Guided waves; Nonlinearity; NDE

INTRODUCTION

NDE is a rapidly growing research field that offers solutions for health assessment of structures. Ultrasonic NDE is usually known for its applications to quantify some basic mechanical and structural properties of solids and it can be used for flaw detection, dimensional measurements and material characterization [1]. Over the last three decades, the ultrasonic guided waves NDE techniques have been enthusiastically discussed for the large detection. Consequently, these have been a subject of much study [2-5]. Ultrasonic guided waves have been of great interest to engineers and scholars because they render a number of practical merits over conventional local point-by-point inspection techniques. They include possibilities of inspecting a large-scale structural integrity at a distance from a fixed transducer position without scanning. However, for linear guided wave NDE, ultrasonic wave propagates through the tested materials, if there is a discontinuity in the wave path, such as crack or flaw, some part of the energy is reflected back and this reflected wave signal is transformed back into electrical signal by the transducer and displayed on the system screen. Thus, the use of linear guided waves is not useful and versatile NDE method for micro-damage detection.

The use of nonlinear acoustics in solid media can be significant for NDE for the interrogation of micro-damages in materials at early stage [6-10]. In other words, the sensitivity of nonlinear acoustic methods for the detection or evaluation of material damage is far higher than that of linear ones. Thus, the nonlinear ultrasonic method can be used as a promising technique in solid media for micro-damages detection [11-13]. With the high sensitivity of the nonlinear ultrasonic approach and the advantages of guided wave techniques illustrated in the above, the nonlinear ultrasonic guided waves have drawn significant attentions for material characterization and micro-damage detection [14-19]. In this paper, some key concepts for success will be introduced along with recent accomplishments including nonlinear guided wave imaging and application to composites.

THEORETICAL CONSIDERATIONS

Compared with bulk waves, second harmonic fields of guided waves are much more complex because of dispersion and their multi-modes nature. In general, ultrasonic guided wave propagates as a wave packet containing a number As shown in Fig. 1, the phase velocity of guided wave propagation is dependent on driving frequency, and for a given propagating guided wave mode, the phase velocity is not equal to the group velocity due to its dispersion nature. It is also indicated that there are at least two guided wave modes at a certain driving frequency. That is the

so-called multimode feature of guided waves propagation.
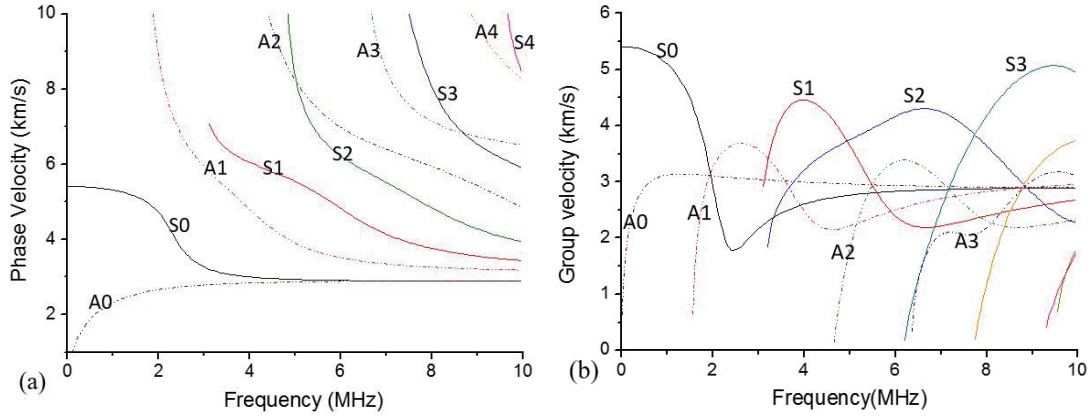
Fig. 1. Phase velocity (a) and group velocity (b) dispersion curves of guided waves in an aluminum plate with 1mm thickness.

In general, the effect of second harmonic generation is weak due to the dispersive nature of Lamb waves. The multi-modes feature of Lamb mode makes it difficult to excite pure single mode experimentally. Consequently, proper mode tuning with physically based features is highly demanded to enhance the efficiency of nonlinear guided wave generation and reception. An investigation of second harmonic generation of guided waves in isotropic plates has been first reported by Deng [20, 21] and de Lima, et al. [22]. A. Srivastava, et.al reported the possibility of existence of anti-symmetric or symmetric Lamb modes at higher harmonics [23]. It is found that the second harmonic amplitude of Lamb modes grows linearly with propagation distance under a certain conditions including "phase matching" and nonzero power flux from the fundamental Lamb wave mode to the second harmonic Lamb waves.

To analyze the second order solution of Lamb wave propagation, perturbations and normal model analysis methods were used [20-24]. Total second harmonic field can be written as

$$\mathbf{u}_2 = \frac{1}{2}\sum_m A_m(z)\mathbf{u}_m(y)\exp(-j2\omega t),$$

(1)

The solution of equation (17) with the source condition $\mathbf{u}_2 = 0$ at $z = 0$ is

$$A_m = \overline{A}_m(z)e^{2jkz} - \overline{A}_m(0)e^{-jk_n^* z},$$

(2)

and

$$\overline{A}_m(z) = \frac{j(f_n^{surf} + f_n^{vol})}{4p_{mn}(k_n^* - 2k)}, \quad k_n^* \neq 2k,$$

(3)

$$\overline{A}_m(z) = \frac{(f_n^{surf} + f_n^{vol})}{4p_{mn}}z, \quad k_n^* = 2k.$$

(4)

where $\mathbf{u}_2$ is the displacement field function, z is the wave propagation direction. $A_m(z)$ is the corresponding expansion coefficient, which is the second order modal amplitude to be determined. The multiplier of 1/2 is included to ensure real quantities. The terms f_n^{surf} and f_n^{vol} are defined as the complex external power due to the surface traction and the volume force, respectively.

Based on the above analyses, it is found that second harmonic amplitude grows linearly with propagation direction, when $k_n^* = 2k$ (synchronism) and $f_n^{surf} + f_n^{vol} \neq 0$ (nonzero power flux). If the selected wave mode satisfies these two conditions, the second harmonic amplitude will have cumulative effect versus propagation

distance. Even a series of double frequency wave components will be generated by the driving sources of nonlinearity. In practice, interest is focused on the second harmonic generation with the cumulative effect as shown in Figure 2, since the cumulative second harmonic play a dominant role in second harmonics field after a certain propagating distance.
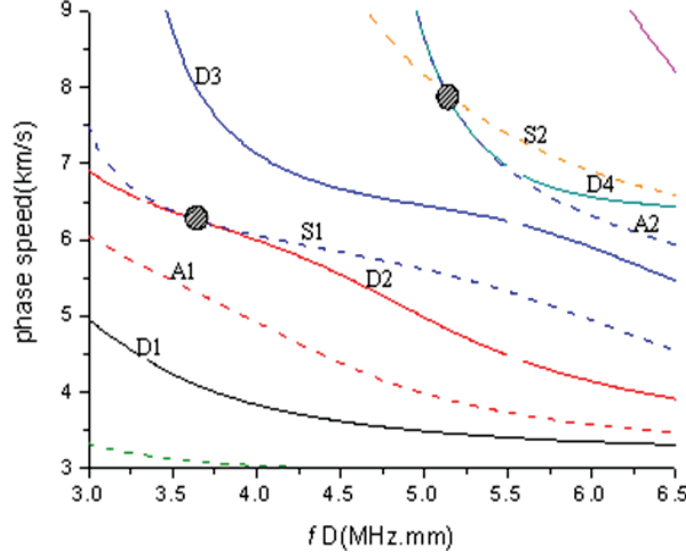
Fig.2 Dispersion curve of fundamental Lamb waves and the phase matched symmetric second harmonic Lamb waves

Even phase matching and non-zero power flux conditions can be used to generate cumulative second harmonic waves, among all of the phase-matched guided waves, the clear guideline for choosing the better phase-matched modes is still obscure. Selecting certain modes from all phase matched ones can play a significant role to improve the sensitivity of the detection of material nonlinearity. Thus, Li, et al. studied the nonlinear feature of phase matched Lamb wave modes for the comparison of efficiency of second harmonic generation [25].

The nonlinear parameter for symmetric Lamb wave modes can be represented by in-plate displacement on the surface as:

$$\beta_{L.s} = \frac{A_2}{A_1^2} \frac{8}{k_l^2 x} \frac{\cosh^2(ph)}{\cosh(2ph)} (1 - \frac{k^2 + q^2}{2k^2}), \tag{5}$$

where A_2 and A_1 are the in-plate displacement amplitude of the second harmonic mode and the primary wave mode with symmetric feature. The nonlinear parameter for anti-symmetric modes can also be derived with the same procedure as:

$$\beta_{L.a} = \frac{A_2}{A_1^2} \frac{8}{k_l^2 x} \frac{\sinh^2(ph)}{\cosh(2ph)} (1 - \frac{k^2 + q^2}{2k^2}). \tag{6}$$

Using the same method, the nonlinear parameters of the Lamb wave can be represented by the out-of-displacement on the surface as

$$\beta_{L.s} = \frac{A_2}{A_1^2} \frac{i8}{k_l^2 x} \frac{p}{k} \frac{\sinh^2(ph)}{\sinh(2ph)} (1 - \frac{2k^2}{k^2 + q^2}), \tag{7}$$

$$\beta_{L.a} = \frac{A_2}{A_1^2} \frac{i8}{k_l^2 x} \frac{p}{k} \frac{\cosh^2(ph)}{\sinh(2ph)} (1 - \frac{2k^2}{k^2 + q^2}). \tag{8}$$

where $\beta_{L.s}$ and $\beta_{L.a}$ are the nonlinear parameters for the symmetric and anti-symmetric Lamb modes respectively. It is important to note that the cumulative second harmonic filed is symmetric even if the primary wave mode is anti-symmetric.

The formulas of the nonlinear parameter for the Lamb wave mode show that, the acoustic nonlinear parameter

for Lamb waves is a function of frequency, material properties and geometric information of the waveguide. The nonlinear features of Lamb modes can be affected by the mode type, frequency of the incident signal, material properties and the geometric information of the waveguide. For a given specimen, if we want to test the material nonlinearity by using Lamb wave modes, the model based nonlinear guided wave technique is necessary for higher efficient data acquisition of second harmonics. As shown in the following dispersion curves, in this work, we compare three different phase matching wave modes, S1 mode at frequency of 3.58MHz, S2 mode at 5.05MHz and A2 mode at frequency of 5.05MHz. The nonlinear features among all these phase matching modes can be calculated as shown in Figure 3.

Experimental work was introduced to verify the nonlinear feature of different Lamb modes. Specimen is aluminum with 1mm thickness. Longitudinal wave speed is 6.35km/s, 3.1km/s for that of transverse wave. According to [83], the material inherent nonlinearity of this material is 5.67. The three "phase matching" modes we chosen in this study are shown in figure 4.6. For a given specimen, if we want to test the material nonlinearity by using Lamb wave modes, the model-based nonlinear guided wave technique is necessary for higher efficient data acquisition of second harmonics as shown in the dispersion curves. In this work, we compare three different phase matching wave modes, S1 mode at frequency of 3.58MHz, S2 mode at 5.05MHz and A2 mode at frequency of 5.05MHz.
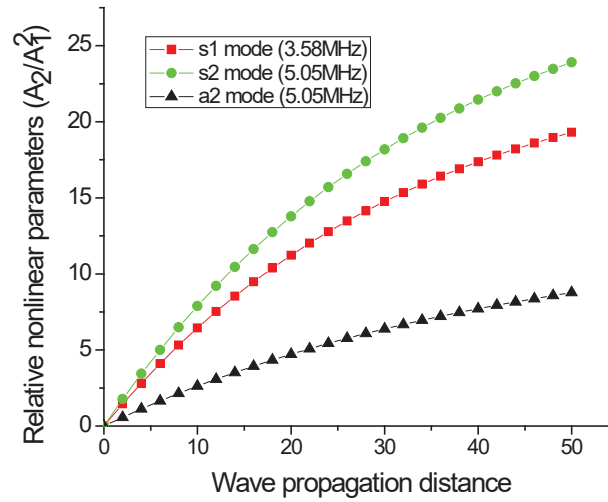

**Fig.3** The nonlinear features of three different phase matching Lamb mode.

NONLINEAR GUIDED WAVES NDE

NDE in Metallic Pipe

Three Al-6063 pipe specimens are used in this work [26]. All the specimens have same dimensions of outer diameter 20mm, the length 400mm, and the thickness is 3mm. they are delivered by the same supplier. In order to induce thermal fatigue into the specimens, especially in early stage, thermal cycles are controlled limited, the temperature and time of thermal fatigue is also controlled strictly. Two of specimens are subjected to 5, 10 cycles of heat fatigue loading, respectively. In one heat-loading cycle, the pipe specimen is heated in a heating furnace at 240^0C temperature for 15 minutes, and then be kept in room temperature (20^0C) for another 15 minutes.

For generating accumulative second harmonic waves, in this work, longitudinal axi-symmetric modes are incident in a metal pipe. To choose the mode pair which satisfies the phase matching condition, we use numerical dispersion curves to find the "phase matching" modes. As shown in Figure 4, the mode pair $(L(0,6), L(0,10))$ is selected in this work for several reasons: 1) theoretically, this mode pair satisfies the phase matching condition, the primary wave mode has the same wave velocity as the secondary mode. 2) for practical consideration, this mode is clearly separated after a certain propagation distance to avoid spurious contributions to the second harmonic wave amplitude by other modes, from the numerical dispersion curve, at the frequency multiplied thickness of 5.05 MHz·mm, when $L(0,6)$ mode is generated, $L(0,5), L(0,7)$ mode could be generated meanwhile, but as

shown in figure 6.2(b), the group velocity of the $L(0,6)$ mode is quite different from that of the $L(0,5), L(0,7)$ mode, so after a certain propagation distance, wave-packs of $L(0,6)$ and $L(0,5), L(0,7)$ modes will separate finally. The mode pair ($L(0,6)$, $L(0,10)$) also satisfies the "group matching" condition, which physically ensures the energy transfer from the fundamental wave consistently.
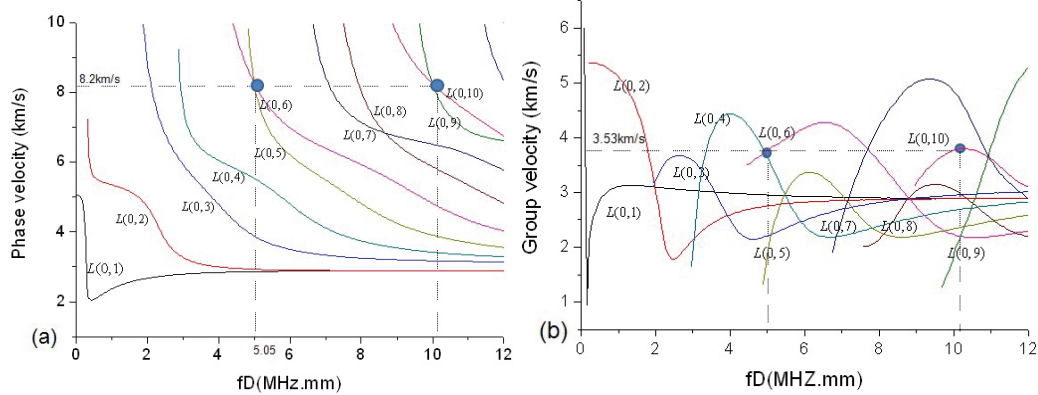

Fig.4 Numerically dispersion curves of Aluminum -6063 pipe: (a) phase velocity versus frequency; (b) group velocity versus frequency [26].

Figure 5 shows the typical waveform of a received signal and its spectrum. The received time-domain signal is processed in the frequency domain with the Fast Fourier transform (FFT) to obtain its spectrum. A_1 and A_2 are determined from the spectrum at the fundamental frequency (1.68 MHz) and the second harmonic frequency (3.36 MHz), respectively.
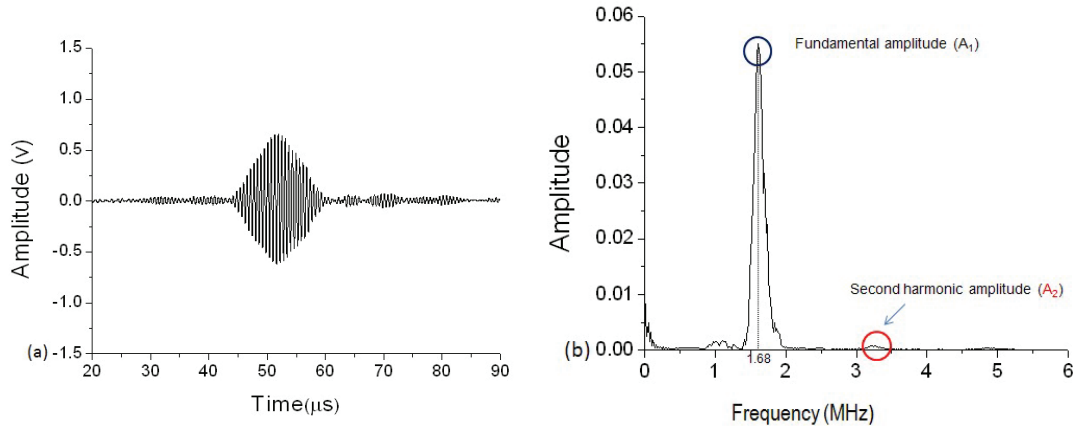
Fig.5 Typical received signal: (a) time domain signal, (b) Fourier spectra of the fundamental and second harmonic signal [26].

The ultrasonic signals are saved for the calculation of the relative nonlinear parameter after wave propagation of 130mm distance. This measurement procedure is conducted three times on the specimen. The values of relative nonlinear parameters increase as propagation distance. Variation of measured acoustic nonlinearity of the OD20mm Al-6063 pipe under different heat-loading cycles is shown in Figure 6. The slope ratio of measured relative nonlinear parameter with respect to wave propagation distance becomes greater when the specimen is subjected to higher heat-loading cycles. This figure shows the quantitative relationship between nonlinearity and heat-loading cycles, thus it can be concluded that nonlinear guided wave is a promising potential method for the diagnostics and prediction of micro-damages in a tube-like structure. This result demonstrates that nonlinear ultrasonic measurements are very useful in quantitatively characterizing the thermal fatigue damage in early stage.
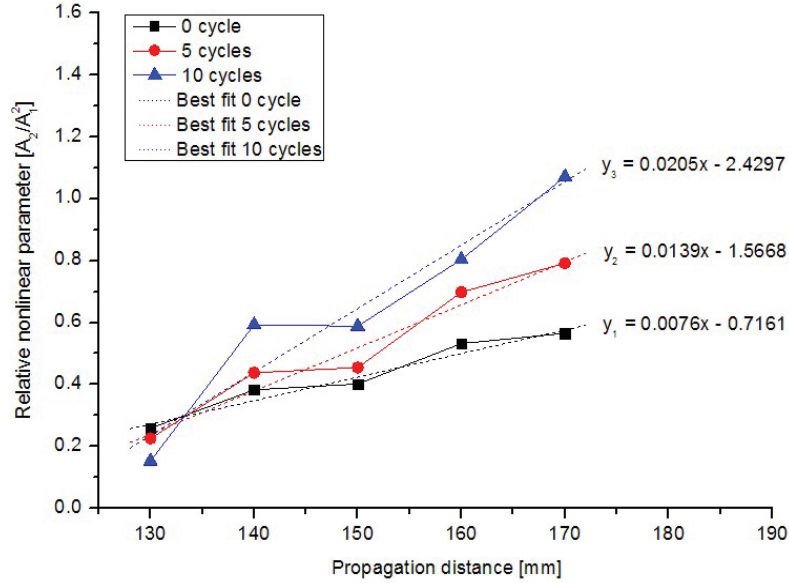
Fig.6 The variation of slope ratio between relative nonlinear parameter (A2 /A12) and propagation distance for the specimens with different thermal fatigue cycles [26].

NDE in Composites

The specimens used in this study are unidirectional and symmetric quasi-isotropic carbon/epoxy laminates with stacking sequences $[0]_6$. The thickness of all specimens is 1.0 mm. The dimensions are 400 mm × 400 mm. Thermal fatigue was imposed on the specimens to cause thermal degradation. The maximum and minimum temperatures of the thermal cycle are 70°C and -55°C, respectively, with a constant cooling and heating time of 15 minutes. The test specimens in this study were subjected to 100, 200, 1000 thermal fatigue cycles [27].

As shown in the Figure 7, the S1mode at frequency 2.25 MHz with phase velocity 9.6 km/s is chosen as a fundamental frequency mode in the present investigation, because this mode satisfies the phase matching condition. Under this condition, a double frequency Lamb mode (S2 mode) is likely generated via the cumulative effect. The double frequency Lamb wave driven by the fundamental S1 mode has the same phase velocity and group velocity as the fundamental frequency wave like the case of longitudinal wave and surface wave propagation. In this work, primary mode (S1 mode) and double frequency Second harmonic Lamb mode (S2 mode) can be taken as a mode pair.
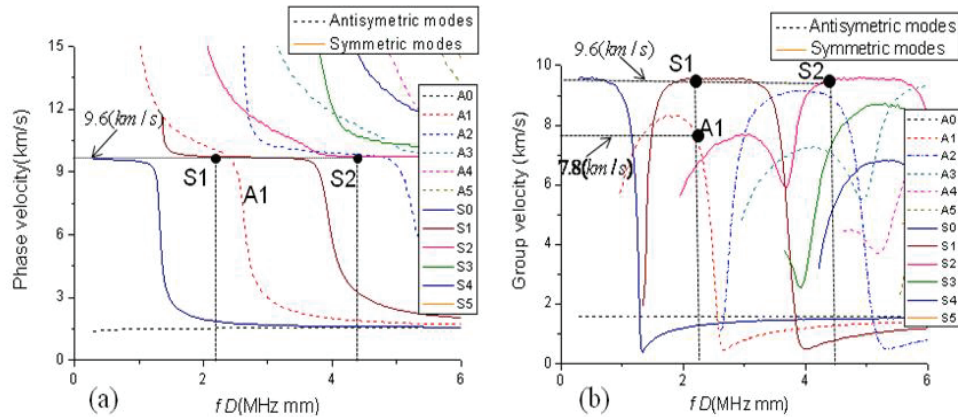
Fig. 7 Phase velocity (a) and group velocity (b) dispersion curves for Lamb wave in $[0]_6$ carbon/epoxy laminates, the propagation direction of the waves is along the fiber direction [27].

In this investigation, the S1-S2 mode wave packet is well separated from the one of A1 with 15cm

propagation distance. Therefore, the frequency spectrum analysis to filter out the second harmonics is conducted within the time gate placed over the S1-S2 wave packet, maintaining propagation distance as 15 cm to avoid the influence of A1 and other modes. A typical Lamb wave signal, generated and detected with wedge transducers is shown in Figure 8, the measured time domain signal was processed by fast Fourier transform (FFT) to get the frequency spectrogram. In the frequency spectrogram, it shows the amplitude of fundamental S1 Lamb mode (A_1) and double frequency second harmonic S2 mode (A_2).
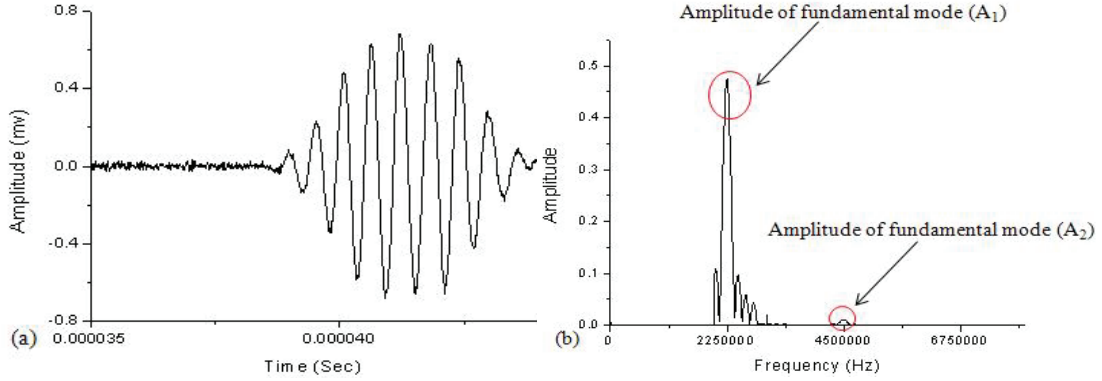

Fig. 8 (a) Typical time-domain signal (b) frequency spectrogram resulted by FFT [27].

To ensure that the measurements from the specimens are not due to the one arising from the measurement system uncertainty, but due to the damage-induced nonlinearity, the demonstration of this cumulative effect is essential. The normalized second harmonic amplitudes (A_2 / A_1^2) have been measured at several different distances as illustrated in Figure 9.
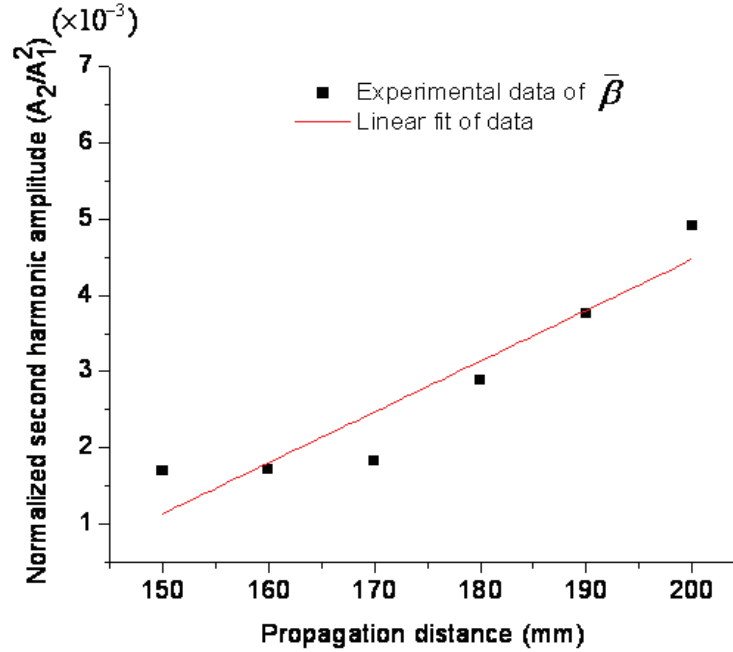

Fig. 9 Variation of the normalized second harmonic amplitude
as a function of propagation distance [27].

Consequently, the linear increment ratio (slope) of the acoustic nonlinearity with wave propagation distance is used to represent the relative acoustic nonlinearity parameter. This method helps to minimize other nonlinearity from couplant and instrument. Figure 9 shows the correlation of the thermal cycles and the relative nonlinear parameters for different specimens. As the thermal cycles increase, the values of acoustic nonlinearity change significantly.
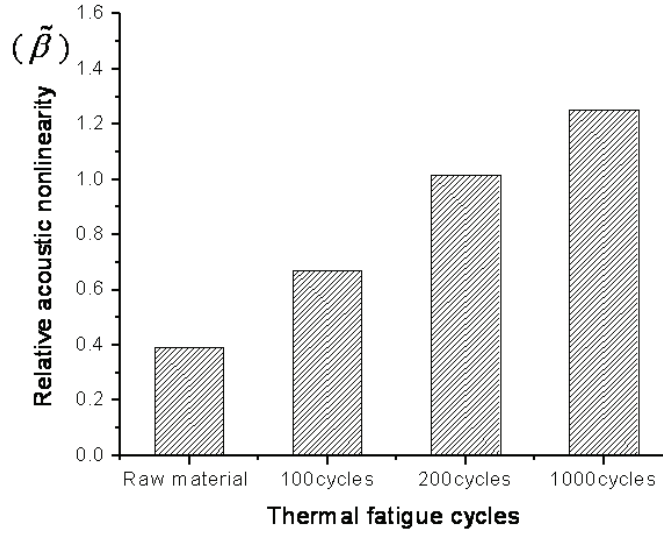
Fig.10 Relative acoustic nonlinearity as a function of thermal cycles [27].

IMAGES OF MICRO-DAMAGE BY NONLINEAR GUIDED WAVES

Another remarkable progress in guided wave NDE is an imaging potential over a hidden or inaccessible damage zone. One of the most effective ways to quantitatively monitor a structure is to obtain an image via either scanning or tomography. The objective of this content is to introduce a nonlinear ultrasonic wave tomography approach to image micro-damage by using RAPID tomography technique. Aluminum alloy-5052 plates of 10mm thickness with tiny corrosions are used in this work. Firstly, the surface wave nonlinearity measurement is introduced to test chemical corrosion induced nonlinearity. Then, the application of RAPID tomography technique is introduced, the attenuation coefficients of primary waves and double frequency surface waves are tested to calculate the defect shape factor γ.

In this work, linear guided waves based tomographic approach is firstly employed to generate the images of micro-corrosive defects [28]. As shown in Figure 10, it is hard to figure out any difference between the linear time domain signals that propagate through the regions with and without tiny chemical corrosive defects. The value of calculated SDC approximately equals zero when the linear time domain signal is employed in conventional tomography algorithm. So, tomographic image by conventional linear time domain signals could not present any information of micro-corrosive defects.
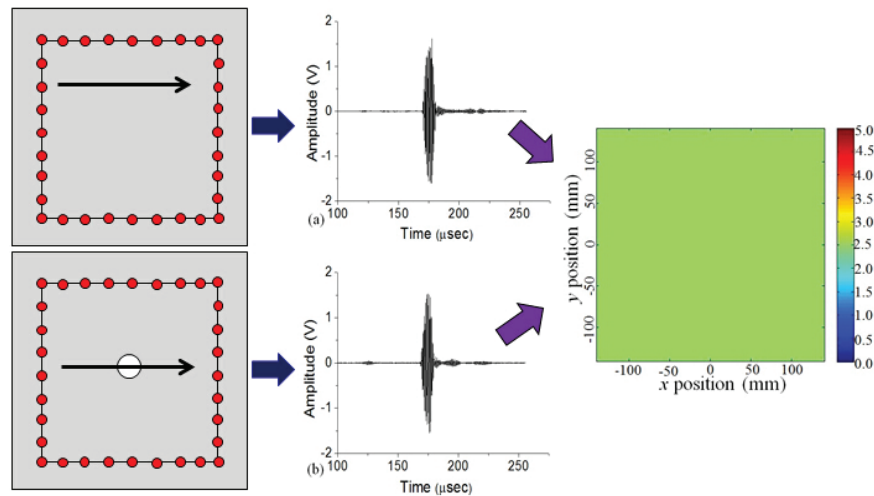

Fig. 11 Conventional ultrasonic tomography based on linear time domain signals [28]

Nonlinearity Measurement

The sensitivity of nonlinear ultrasonic methods to the damages features is far greater than that of linear acoustic approach. Measured nonlinearity should include damage-induced nonlinearity plus any nonlinearity from instrumentations and couplant. To assure that the nonlinearity from material damage is dominated over other sources. Only the nonlinear parameters noticeable exceeding the baseline value of the raw specimens without damages after obtained over a number of times, and the average data is plotted to alleviate the experimental uncertainly. Figure 11 shows the typical waveform of a received signal and its frequency spectrum. The received time-domain signal is processed in the frequency domain with the Fourier transform to obtain its spectrum.

The principal difference between linear and nonlinear ultrasonic test is that in the latter the existence and characteristics of defects are often related to an acoustic signal whose frequency differs from that of the input signal [9]. In this investigation, the frequency spectrum analysis to filter out the different frequency components is conducted. Nonlinear frequency components are used to calculate the SDC value in the tomographic algorithm.
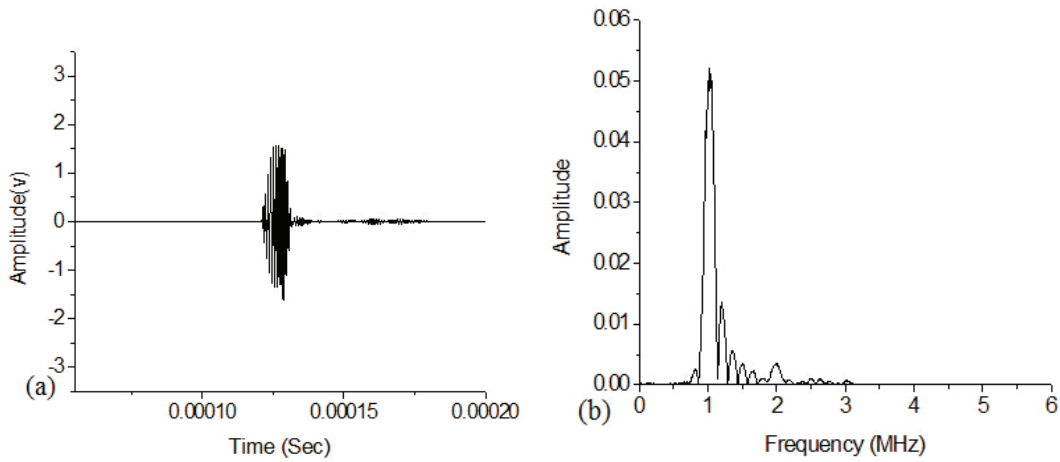
Fig. 12 Typical received signal: (a) time domain signal, (b) frequency spectra of the fundamental and second harmonic signal [28].

For nonlinear guided wave test, nonlinear responses of higher harmonic generation which induced by instruments, coupling media as well as ambient noise are inevitable. To ensure that what is measured from the specimens is mainly due to the nonlinearity induced by the micro-damages rather than arising from the measurement system, demonstration of this cumulative effect is essential. Wave propagation distance was varied from 50 mm to 250 mm with 25 mm interval and conduct two times. As shown in Figure 12. It is found that the relative nonlinear parameter grows with the propagation distance via the accumulative effect to a certain point when material attenuation becomes dominant.
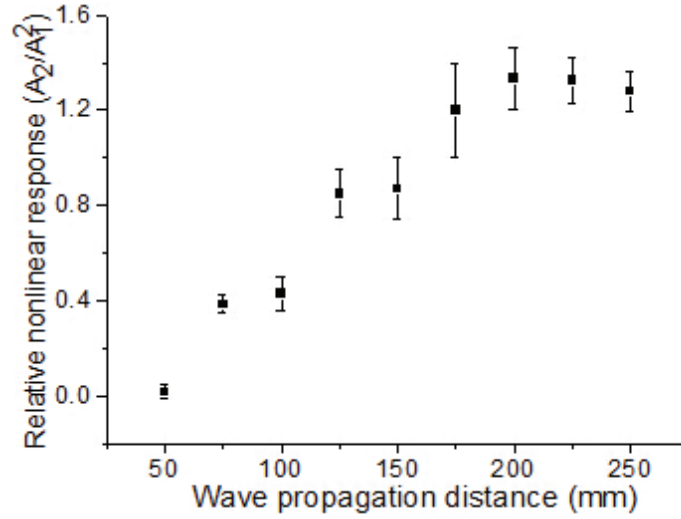
Fig. 13 Cumulative effect of nonlinear response as propagation distance [28].

Images Reconstructed by the Nonlinear Frequency Components

As stated above, in the case of the scattering of an acoustic wave by the micro-crack, the amplitude of the nonlinear acoustic signals can be much greater than the level of those generated in intact media. Considering the nonlinear response of difference frequency components generation when the ultrasonic waves propagate through micro-damaged zone, the frequency domain signals are used to calculate the SDC value in this work. Thus, for nonlinear guided wave tomographic technique, instead of extracting the linear features from a time domain signal, frequency conversion induced by micro-damages of guided wave signals in frequency domain is used in the modified nonlinear tomographic algorithm.

The time domain Rayleigh surface wave signal was transformed into frequency spectrums to analyze the frequency conversion induced by micro-defect. Measured nonlinear acoustic signals in frequency domain was reconstructed by the modified RAPID algorithm to illustrate the tomographic image. Figure 13 demonstrates the ability of the modified tomographic algorithm with the nonlinear surface wave signal to express the micro-defect region by image. The most significant variation in the SDC is observed approximately in the middle of the damage zone. There are also other zones of the tomogram that depict changes in the SDC that can not be explained via a change in the material micro-defects in those zones. These anomalies includes the noise sources for the change in SDC include inconsistent sensor grounding, A/D jitter, and reproducibility of the gated sinusoid used to excite the sensors.
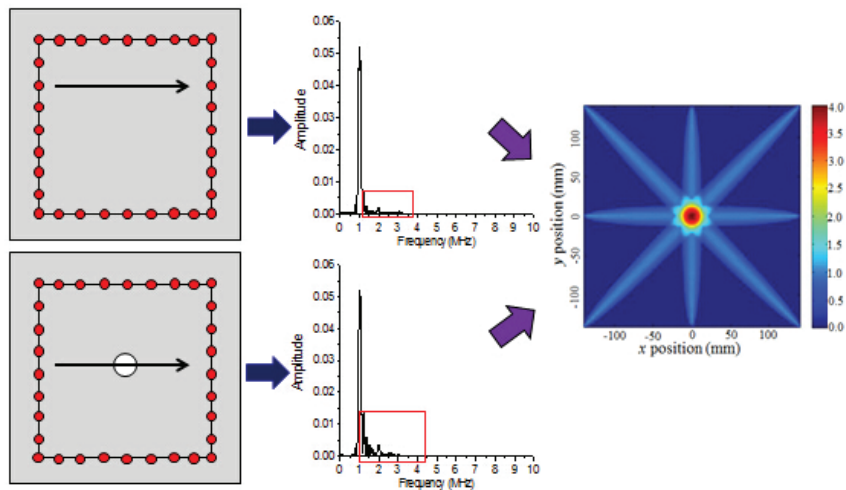

Fig. 14 Modified nonlinear ultrasonic tomography based on frequency domain signals [28].

CONCLUSIONS

Proper mode tuning with physically based features is highly demanded to enhance the efficiency of nonlinear guided wave generation and reception. Nonlinear feature among different guided wave modes provides a higher efficient method to choose guided wave modes to detect micro-damages by using nonlinear guided wave technique. The use of phase matched guided wave modes in metallic and composite materials for NDE of material degradation shows the potential application of measured nonlinear parameter of guided waves as an effective tool to evaluate material damage at early stage.

REFERENCES

1. J. Blitz, G. Simpson, *Ultrasonic methods of non-destructive testing*, Springer, London, 1996.
2. J. D. Achenbach, *Wave propagation in elastic solids*, Elsevier, New York, 1975.
3. I. A. Viktorov, *Rayleigh and Lamb waves physical theory and application*, Plenum, New York, 1967.
4. J. L. Rose, "A baseline and vision of ultrasonic guided wave inspection potential", *Journal of Pressure Vessel Technology*, **124**:273-282, (2002).
5. D. N. Alleyne, P. Cawley, "The intersection of Lamb waves with defects", *IEEE transaction on ultrasonics, ferroelectrics and frequency control*, **39**:381-397, (1992).
6. J. H. Cantrell, W.T. Yost, "Nonlinear ultrasonic characterization of fatigue microstructures", *International Journal of Fatigue*, **23**:487-490, (2001).
7. P. B. Nagy, "Fatigue damage assessment by nonlinear ultrasonic material characterization", *Ultrasonics*, **36**:275-381, (1998).
8. Van Den Abeele, K. E. -A., P. A. Johnson and A. Sutin, "Nonlinear Elastic Wave Spectroscopy (NEWS) Techniques to Discern Material Damage, Part I: Nonlinear Wave Modulation Spectroscopy (NWMS)", *Research in Nondestructive Evaluation*, **12(1):** 17–30, (2000).
9. Van Den Abeele, K. E. –A., P. Y. Le Bas, B. Van Damme and T. Katkowski, "Quantification of material nonlinearity in relation to microdamage density using nonlinear reverberation spectroscopy: Experimental and theoretical study", *The Journal of the Acoustical Society of America*, **126(3):** 963–972, (2009).
10. W. Li, Y. Cho and S. Hyun, "Characteristics of ultrasonic nonlinearity by thermal fatigue", *International Journal of Precision Engineering and Manufacturing*, **13**:935-940, (2012).
11. W. Li, Y. Cho and J. D. Achenbach, "Assessment of heat treated Inconel X-750 alloy by nonlinear ultrasonics", *Experimental Mechanics*, **53(5):**775-781, (2013).
12. K. Y. Jhang, "Applications of nonlinear ultrasonics to the NDE of material degradation". *IEEE transactions on ultrasonics, ferroelectrics, and frequency control*, **47(3):** 540–548, (2000).
13. D. Yan, B. W. Drinkwater, S. A. Neild, "Measurement of the ultrasonic nonlinearity of kissing bonds in adhesive joints", *NDT&E International*, **42**: 459-466, (2009).
14. K. H. Matlack, J. Y. Kim, L. J. Jacobs, J. Qu, "Experimental characterization of efficient second harmonic generation of Lamb wave modes in a nonlinear elastic isotropic plate", *Journal of Applied Physics*, **109**:014905, (2011).
15. M. F. Muller, J. Y. Kim, J. Qu, L. J. Jacobs, "Characteristics of second harmonic generation of Lamb waves in nonlinear elastic plates", *Journal of the Acoustical Society of American*, **127**:2141-2152, (2010).
16. M. Deng, J. Pei, "Assessment of accumulated fatigue damage in solid plates using nonlinear Lamb wave approach", *Applied Physics Letters*, **90**:121902, (2007).
17. C. Pruell, J. Y. Kim, J. Qu, L. J. Jacobs, "A nonlinear-guided wave technique for evaluating plasticity-driven material damage in metal plate", *NDT&E International*, **42**:199-203, (2008).
18. C. Bermes, J. Y. Kim, J. Qu, L. J. Jacobs, "Nonlinear Lamb waves for the detection of material nonlinearity", *Mechanical Systems and Signal Processing*, **22**:638-646, (2008).
19. N. Matsuda, S. Biwa, "Phase and group velocity matching for cumulative harmonic generation in Lamb waves", *Journal of Applied Physics*, **109**, 094903, (2011).
20. M. Deng, "Cumulative second harmonic generation of Lamb mode propagation in a solid plate", *Journal of Applied Physics*, **85**:3051-3058, (1999).

21. M. Deng, "Analysis of second harmonic generation of Lamb modes using modal analysis approach", *Journal of Applied Physics*, **94**:4152-4159, (2003).
22. W. J. N.de Lima, M. F. Hamilton, "Finite-amplitude waves in isotropic elastic plates", *Journal of Sound and Vibration*, **265**: 819–839, (2003).
23. A. Srivastava, F. L. di Scalea, "On the existence of antisymmetric or symmetric Lamb waves at nonlinear higher harmonics", *Journal of Sound and Vibration*, **323**:932-943, (2009).
24. B. A. Auld, *Acoustic fields and Waves in Solids*, Malabar, Kreiger Press, 1973
25. W. Li, Y. Cho, J. D. Achenbach, *Rev Prog Quant Nondestr Eval,* **1581** 662, 2010.
26. W. Li, Y. Cho, "Thermal fatigue damage assessment in an isotropic pipe using nonlinear ultrasonic guided waves", *Experimental Mechanics*, **54(8):** 1309-1318, (2014).
27. W. Li, Y. Cho, J. D. Achenbach, "Detection of thermal fatigue in composites by second harmonic Lamb waves", *Smart Materials and Structures*, **21(8):**085019, (2012).
28. W. Li, Y. Cho, "Combination of nonlinear ultrasonics and guided wave tomography for imaging the micro-defects", *Ultrasonics*, **65**:87-95, (2016).